Supporting information - Critical slowdown of spontaneous fluctuations in the vicinity of metal-insulator transition in rare earth nickelates

Nanna Zhou Hagström,[1,*] Meera Madhavi,[1] Emma Bernard,[1] Nushrat Naushin,[1] Jugal Mehta,[1] Pooja Rao,[1] Surya Botu Teja,[1] Ravindra S. Bisht,[2] Tae Joon Park,[3] Ranjan Patel,[2] Toyanath Joshi,[4] Sophie A. Morley,[5] Sujoy Roy,[4,5,6] Xiaoqian M Chen,[7] Andrei Fluerasu,[7] David Lederman,[4] Shriram Ramanathan,[2] and Roopali Kukreja[1,*]

[1]*Department of Materials Science and Engineering, University of California Davis, Davis, California 95616, USA*

[2]*Department of Electrical and Computer Engineering, Rutgers, The State University of New Jersey, Piscataway, NJ, USA*

[3]*School of Materials Engineering, Purdue University, West Lafayette, IN 47907*

[4]*Department of Physics, University of California Santa Cruz, Santa Cruz, California 95064, USA*

[5]*Advanced Light Source Lawrence Berkeley National Laboratory Berkeley, California 94720, USA*

[6]*Materials Sciences Division Lawrence Berkeley National Laboratory Berkeley, California 94720, USA*

[7]*National Synchrotron Light Source II (NSLS-II), Brookhaven National Laboratory, Upton, New York 11973, USA*

SI 1. SAMPLE CHARACTERIZATION INCLUDING ELECTRICAL AND X-RAY MEASUREMENTS

Figure SI 1 shows the resistivity measurements for all three samples used in the main article. The metal-to-insulator transition temperature was defined as the inflection point of the resistivity measurement, while the Néel temperature was obtained using $\mathrm{dln}(\rho)/\mathrm{d}(1/T)$ [1]. From resistivity measurements, we find T_{MIT} = 140 K, T_{Neel} = 88 K for NNO/STO, T_{MIT} = 150 K for NNO/LAO and T_{MIT} = 470 K for SNO/STO (Figure SI 1). For NNO/STO, $T_{Néel}$ obtained from resistivity measurements was compared with temperature dependence of the x-ray magnetic scattering peak as discussed below. For NNO/LAO and SNO/STO, x-ray magnetic scattering was used to determine $T_{Néel}$ around 120 K and 170 K, respectively (see Figure SI 3).

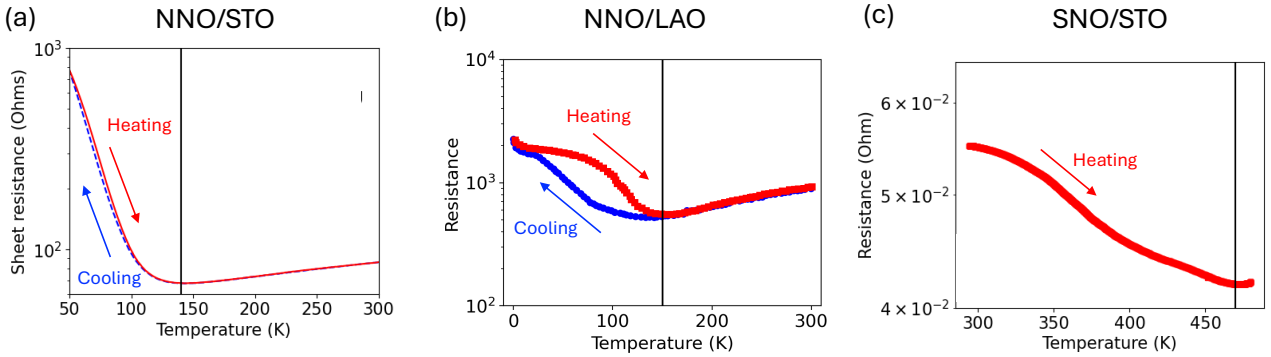

FIG. SI 1. Resistivity measurements for (a) NNO/STO, (b) NNO/LAO and (c) SNO/STO. T_{MIT} is shown by the black line.

The peak parameters of the structural (1/2 1/2 3/2) Bragg peak (position, intensity and correlation length) of the three samples were extracted from a 2D Gaussian fit of the speckle patterns and are plotted as a function of temperature in Figure SI 2. In rare earth nickelates, the (1/2 1/2 3/2) Bragg peak is present in both the insulating and metallic phases. However, the MIT is accompanied by a decrease of the out of plane lattice parameter [2] which is visible in the half order peak [3]. The transition is also accompanied by an intensity increase of the structural peak due to a higher symmetry ordering of the octahedral tilts in the metallic phase [4].

For NNO/STO, the peak position and the intensity follow the same trend, steadily increases until 125K after which they plateau and slowly decrease (Figure SI 2a). The changes observed in intensity and peak position are indicative of phase transition based on x-ray measurements which were found to be about 15 K lower than T_{MIT} from the resistivity data. At 125K, the

* To whom correspondence should be addressed; E-mail: nanna.zh@gmail.com and rkukreja@ucdavis.edu

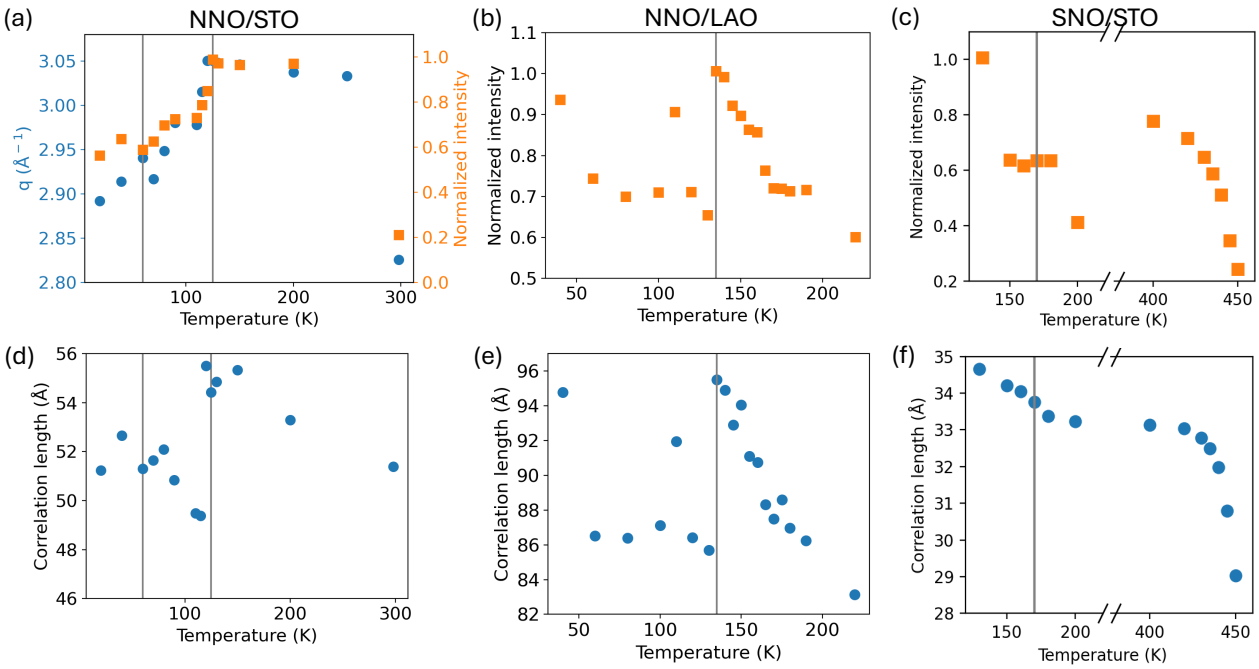

FIG. SI 2. (1/2 1/2 3/2) Bragg peak (position, intensity and correlation length): Normalized intensity for (a) NNO/STO, (b) NNO/LAO and (c) SNO/STO. For NNO/STO, peak position obtained from rocking curves is also included. Correlation length for (d) NNO/STO, (e) NNO/LAO and (f) SNO/STO. The grey lines indicate the temperatures at which slowdown of the fluctuations are observed as dicussed in the main text. For SNO/STO the grey line is at T_{Neel}=170K.

correlation length (=1/FWHM) shows a sharp increase (Figure SI 2d), also consistent with a sudden change of the macroscopic ordering. The x-ray scattering of the magnetic peak shows the onset of the magnetic transition at lower temperatures ($\sim$ 60 K, see SI 3) than calculated from the resistivity measurements where $T_{Neel} \sim 88$ K.

For NNO/LAO, the intensity and correlation length show an increase at 135 K, similar to the trend observed for NNO/STO (Figure SI 2b, e). In this sample, the onset of the structural change was also 15 K below T_{MIT} compared to resistivity mesurements. The presence of the strong LAO peak hindered proper estimation of peak shift of NNO. The temperature dependence of the x-ray magnetic scattering (1/4 1/4 1/4), indicates a magnetic transition temperature of $\sim$120K, which is 30 K below T_{Neel} calculated from the resistivity measurements. An extremely broad low intensity peak is still observed up to 135 K, indicative of a broad magnetic transition with some diffuse magnetic regions surviving up to near MIT.

For SNO/STO, a continous decrease of the intensity from 130K to 450K is observed as shown in Figure SI 2c. Note that the increase in intensity at 400K was due to beamline alignment after lost beam. No sharp changes in correlation length is observed (Figure SI 2f), but as mentioned in main articl, we were not able to reach above T_{MIT} due to experimental constraints at the

beamline.

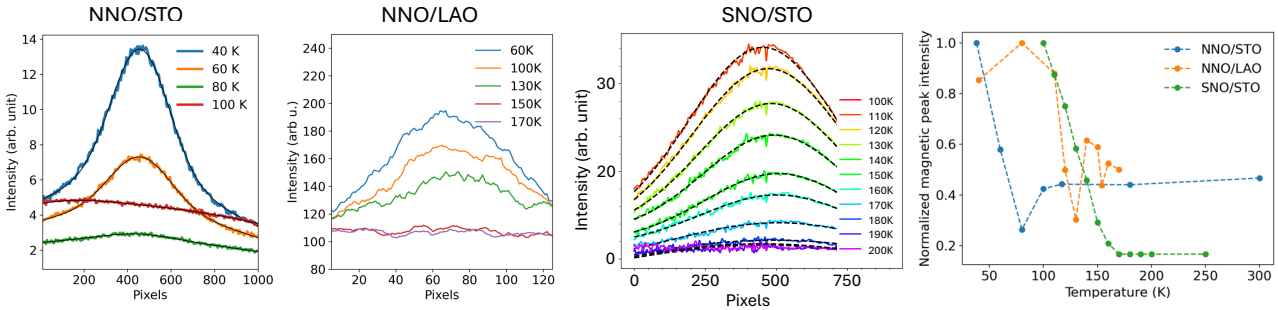

FIG. SI 3. Temperature dependence of x-ray magnetic scattering (1/4 1/4 1/4) peak: Magnetic scattering peak for (a) NNO/STO, (b) NNO/LAO and (c) SNO/STO as a function of temperature. (d) Normalized intensity for all three samples plotted as a function of temperature.

Figure SI 4 shows the $\theta - 2\theta$ scans of the (002) Bragg peak of all three samples.

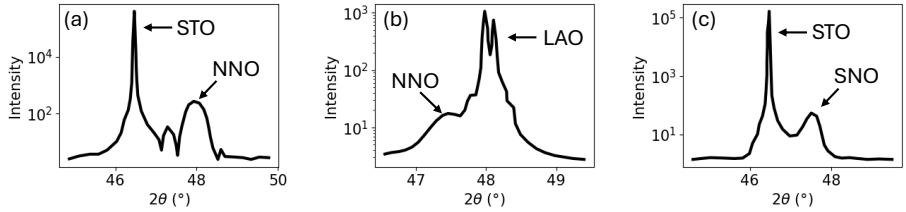

FIG. SI 4. $\theta - 2\theta$ scans of the (002) Bragg peak of (a) NNO/STO, (b) NNO/LAO and (c) SNO/STO.

SI 2. TWO-TIME CORRELATION FUNCTION DATASETS

Two time correlation plots at all temperatures are plotted for NNO/STO, NNO/LAO and SNO/STO in Figures SI 5, SI 6 and SI 7 respectively. We observed non-equilibrium dynamics at all temperatures for all three samples, albeit weakly for the SNO/STO sample. We also note that the data for the NNO films have a much better signal to noise (SNR) than the SNO films, potentially due to experimental conditions.

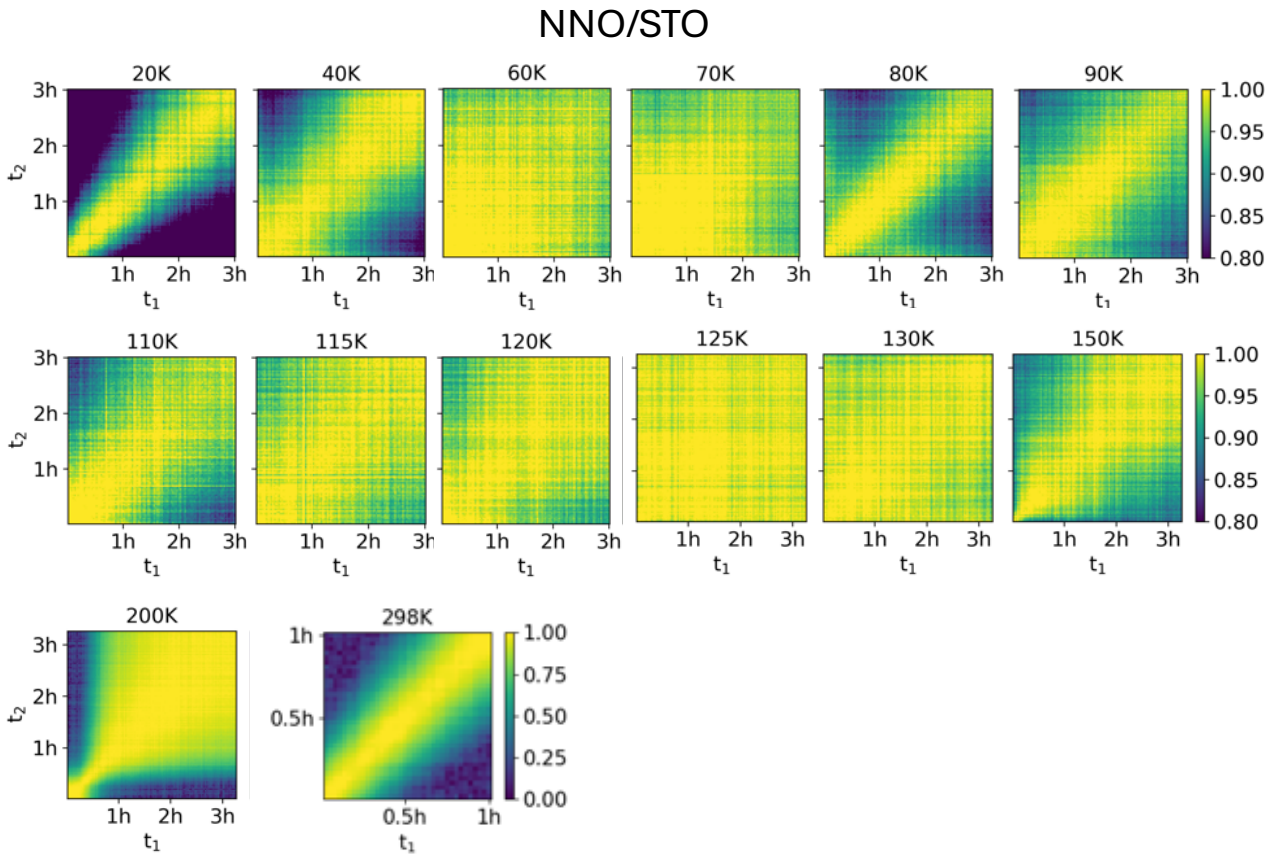

FIG. SI 5. Normalized two-time correlation plots for NNO/STO for all measured temperatures.

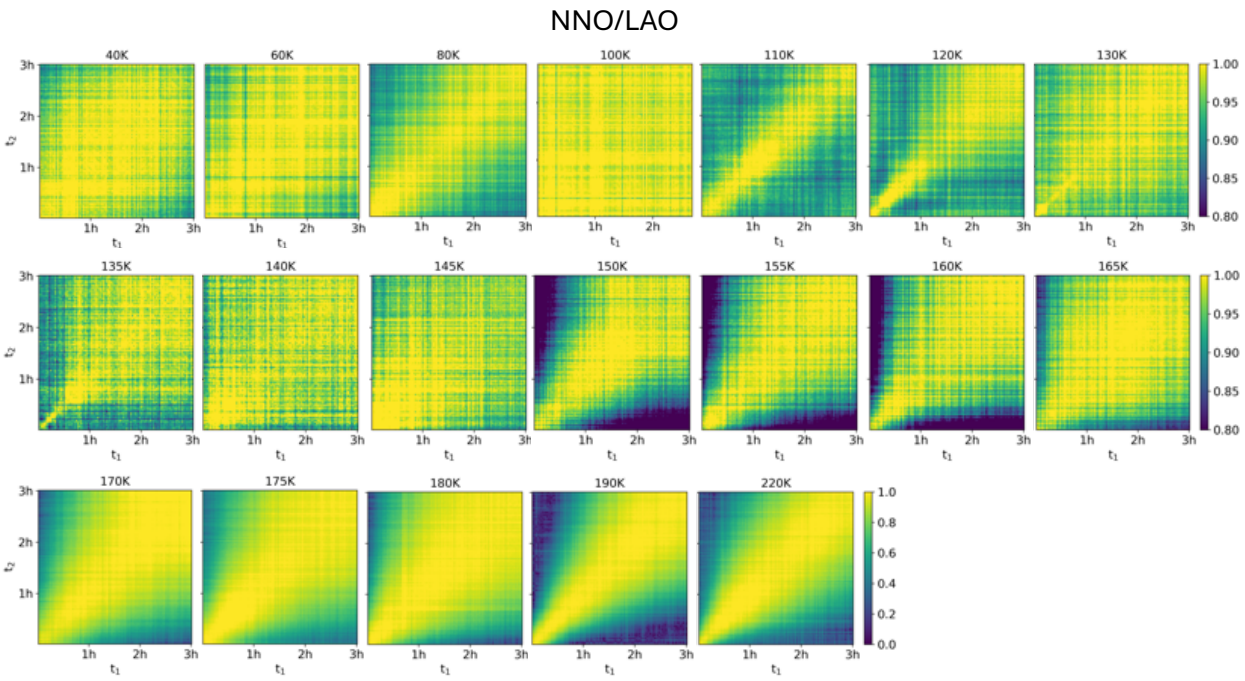

FIG. SI 6. Normalized two-time correlation plots for NNO/LAO for all measured temperatures

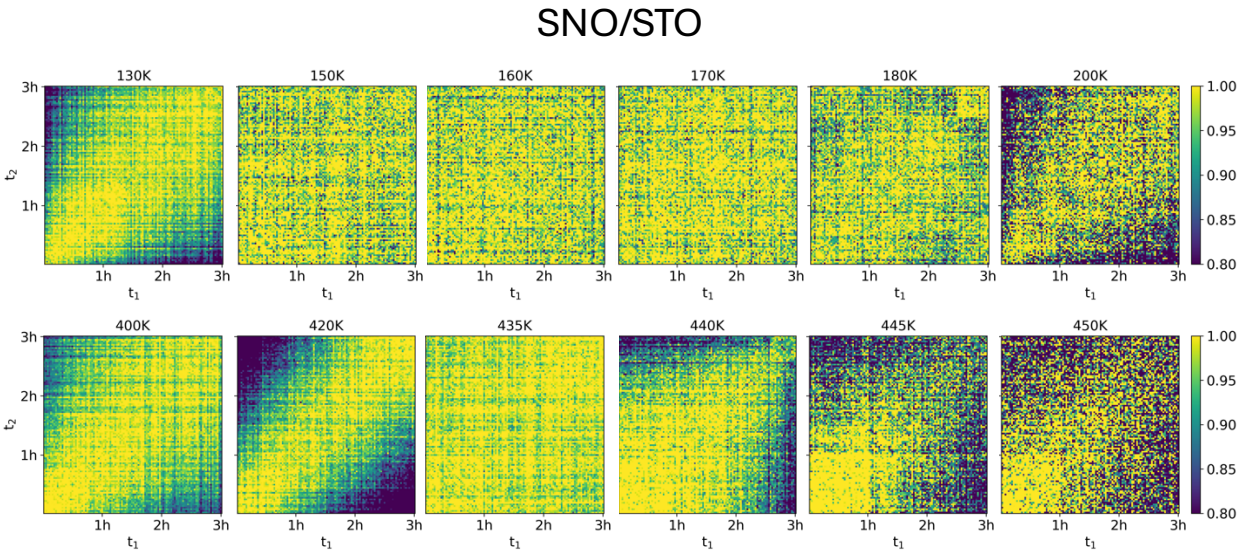

FIG. SI 7. Normalized two-time correlation plots for SNO/STO.

SI 3. INTERMEDIATE SCATTERING FUNCTION DATASETS

Figure SI 8 shows the intermediate scattering function (g_2) obtained at zero wait time for all measured temperatures for (a) NNO/STO, (b) NNO/LAO and (c) SNO/STO. The contrast of the g_2 function are plotted in the insets.

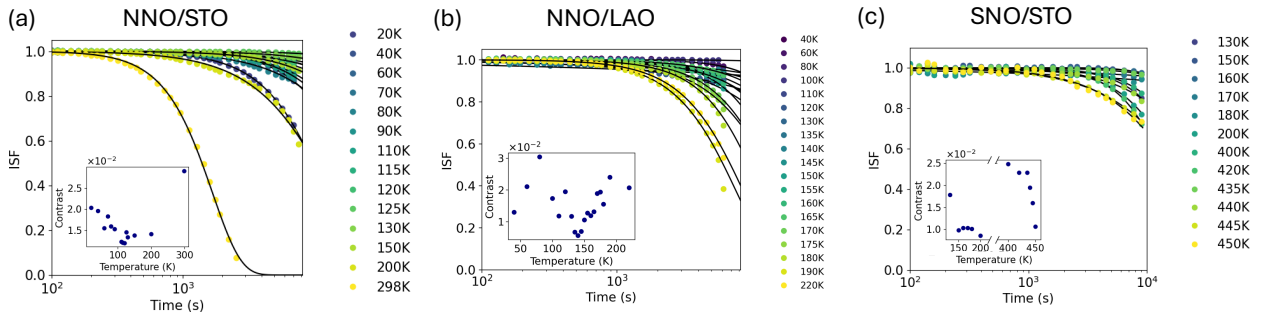

FIG. SI 8. ISF at zero wait time for all measured temperatures for (a) NNO/STO (b) NNO/LAO and (c) SNO/STO. The insets shows the contrast of the g_2 function.

SI 4. NON-EQUILIBRIUM DYNAMICS IN NNO

Figure SI 9 shows the ISF of NNO/LAO at different wait times t_w for (a) 120K and (b) 175K. NNO/LAO behaves in a similar manner as NNO/STO for most of the temperature range except for 110 to 140 K. This is also clear from ISF plotted at at 175K (Figure SI 9b), where the decay constant τ increases with t_w and β remains constant for the entire t_w. However, in 110 to 140 K regime, the shape of the ISF changes as a function of wait time, illustrated by the change in β (inset of Figure SI 9a). Normalized time constants as discussed in main article are also plotted for NNO/LAO in Figure SI 9c. For most temperatures, except 110 to 140 K, the normalized time constant is fitted as discussed in the main article for NNO/STO film. For temperatures 110 to 140 K, the reduced decay constant does not vary exponentially with wait time, and decreases with time and thus was not fitted. The obtained τ^*_{fit} is shown in Figure SI 9d.

Figure SI 10 summarizes decay constants for different wait times as a function of temperature for (a) NNO/STO, (b) NNO/LAO and (c) SNO/STO. For all temperatures for NNO/STO and most temperatures for NNO/LAO, decay constants increase with wait times as discussed in the main article. For NNO/LAO, in the temperature range of 110-140 K, change in β results influences τ and results in a decrease of τ. For SNO/STO, there is no clear trend as a function of wait time, highlighting yet a differences compared to NNO films.

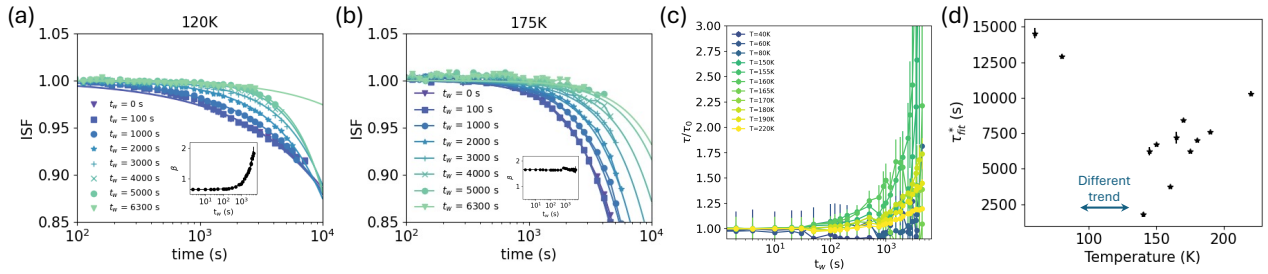

FIG. SI 9. Non-equilibrium behavior of NNO/LAO. ISF for different wait times at (a) T=120K and (b) T=175K. Inset shows β as a function of t_w. (c) Evolution of the normalized decay constant for different wait times showing exponential behavior. (d) obtained τ^*_{fit} as a function of temperature.

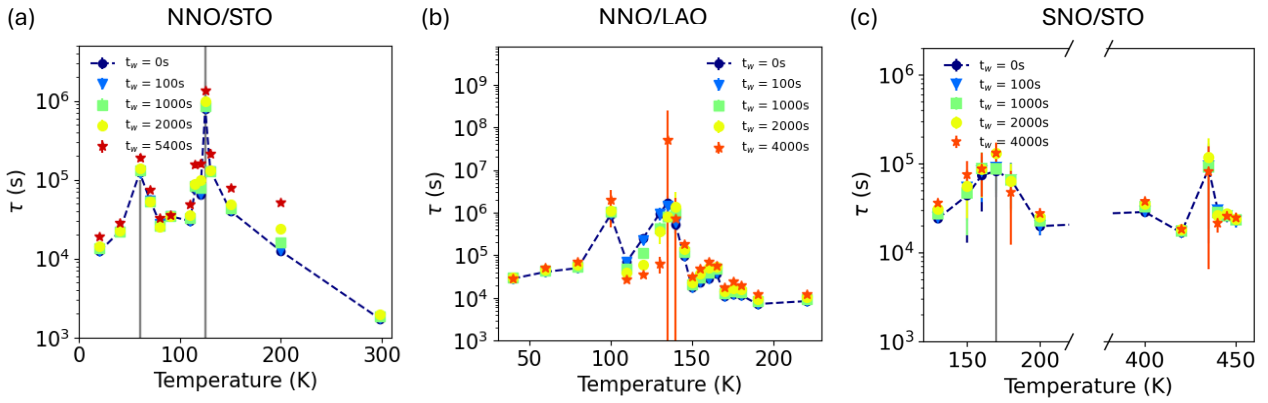

FIG. SI 10. Decay constants at different wait times: Decay constant for (a) NNO/STO, (b) NNO/LAO and (c) SNO/STO, for different wait times and for zero wait time, as a function of temperature

SI 5. Q-DEPENDENCE OF THE FLUCTUATION DYNAMICS

Figure SI 11 shows all measured temperatures for the q-dependence of the fluctuations in NNO/STO. Figure SI 11a presents the decay constant at different wavevectors, clearly showing that the slowdown is observed at higher wavevectors. Figure SI 11b shows the normalized q-dependence for all temperatures as discussed in the main article. These datasets were fitted using, $\tau/\tau_0 = K(q/q_0)^2 - 2(K+\epsilon_1)(q/q_0) + (K+\epsilon_2) \approx K(q/q_0 - (1+\epsilon'))^2$ as discussed in the main article. Figure SI 11b shows the normalized decay constant which is normalized by τ_0 and K, to highlight the obtained quadratic dependence for all measured temperatures.

Figure SI 12 also confirms q-dependence for NNO/LAO. Figure SI 12a shows the q-dependence of the decay constant as function of temperature, clearly indicating that fluctuations slow down at higher q-values. This is also visible from Figure SI 12b which shows the normalized decay constant as a function of q, for selected temperatures. Note that for NNO/LAO peak, only three ROIs were used to obtain good SNR.

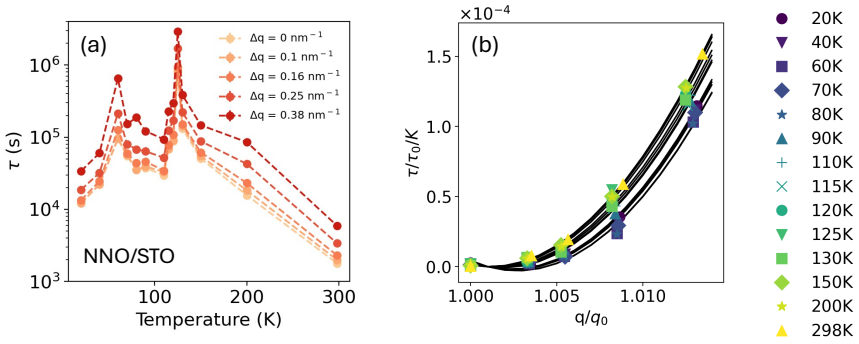

FIG. SI 11. q-dependence of the fluctuation dynamics in NNO/STO: (a) Decay constants τ as a function of temperature for different wavector q. These were obtained by fitting decay constant to ISF obtained from each ROI as shown in Figure 1 of the main article. (b) q-dependence of the normalized decay constant for all measured temperatures. Black curves shows the fit $\tau/\tau_0 = K * (q/q_0 - \epsilon')^2$ and clearly shows quadratic dependence for all temperatures.

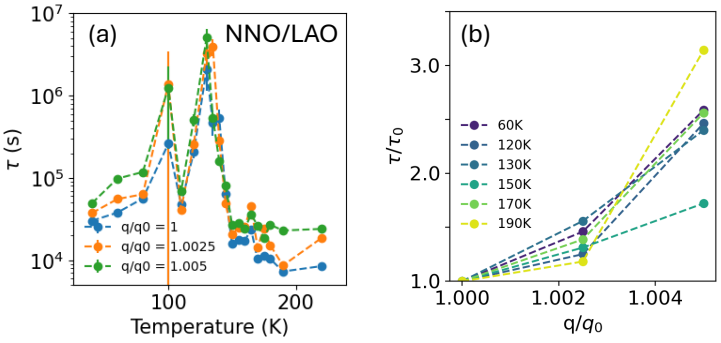

FIG. SI 12. q-dependence of the fluctuation dynamics in NNO/LAO: (a) Decay constants τ as a function of temperature for different wavector q. (b) q-dependence of the normalized decay constant for selected temperatures.

[1] J. Liu, M. Kargarian, M. Kareev, B. Gray, P. J. Ryan, A. Cruz, N. Tahir, Y.-D. Chuang, J. Guo, J. M. Rondinelli, J. W. Freeland, G. A. Fiete, and J. Chakhalian, Nature Communications **4**, 2714 (2013), publisher: Nature Publishing Group.

[2] M. L. Medarde, Journal of Physics: Condensed Matter **9**, 1679 (1997).

[3] J. Mehta, S. Smith, J. Li, K. Ainslie, N. Albayati, T. Joshi, P. Rao, Y.-H. Cheng, S. Jeppson, R. Jangid, E. Karapetrova, D. A. Walko, H. Wen, D. Lederman, and R. Kukreja, Physical Review Materials **7**, 096201 (2023), publisher: American Physical Society.

[4] S. Middey, J. Chakhalian, P. Mahadevan, J. Freeland, A. Millis, and D. Sarma, Annual Review of

Materials Research **46**, 305 (2016).